Free Carrier Generation in Semiconductors Induced by Absorption of Sub-Band Gap Light. A Photoelectrochemical Study with Nanoporous GaP

D. Vanmaekelbergh,* M. A. Hamstra, and L. van Pieterson

Debye Institute, Utrecht University, P.O. Box 80000, 3508 TA Utrecht, The Netherlands

Received: February 24, 1998; In Final Form: June 18, 1998

The main mechanisms of electron−hole generation in a semiconductor induced by absorption of a sub-band gap photon are considered. Electron−hole generation with sub-band gap light involves optical and thermal transitions between delocalized valence or conduction band states and localized band gap states. A semiconductor device with a retrieval layer in which electron−hole pairs are effectively separated is considered. For each mechanism, the steady-state photocurrent quantum yield and the photocurrent response to a harmonic modulation of the intensity of sub-band gap light is calculated. It is shown that sub-band gap intensity modulated photocurrent spectroscopy makes it possible to resolve different contributions to the sub-band gap photocurrent and to study the kinetics of free carrier generation induced by sub-band gap light absorption. Experimental results obtained with nanoporous GaP photoanodes are analyzed; two different mechanisms are responsible for sub-band gap photocurrent flow. The potential of sub-band gap intensity modulated photocurrent spectroscopy for the characterization of (surface) localized band gap states is discussed and illustrated with results obtained with nanoporous GaP.

Introduction

The excitation of electrons from the valence band into the conduction band of an insulator or semiconductor due to absorption of photons with energy larger than the band gap has been studied extensively.[1] The probability of such processes can be understood on the basis of band theory. Less attention has been paid to the absorption of light of energy considerably smaller than the gap. Absorption of sub-band gap photons is necessarily mediated by electronic states located in the band gap. Amorphous semiconductors and insulators have a considerable density of such states, and absorption of sub-band gap photons is important.[2] In pure single crystals, the probability of absorption of sub-band gap photons is generally very low and mainly mediated by localized surface states. However, experiments which probe sub-band gap light absorption in single crystals have been reported.[3] Sub-band gap optical transitions generally lead to one type of free charge carrier (electrons in the conduction band or holes in the valence band). This effect has been explored in photoconductivity and surface photovoltage spectroscopy for the study of the energetic distribution of interfacial states and their cross sections for photon absorption and capture of an electron or hole.[4] Such studies are often performed at low temperature and under vacuum conditions.

A few papers report on the observation of steady-state photocurrent flow in an electrochemical cell with a semiconductor working electrode illuminated with sub-band gap light.[5] In conventional electrochemical studies, with single crystalline semiconductor electrodes having a flat solid/electrolyte interface, the sub-band gap photocurrent quantum yield (the photocurrent density divided by the product of the elementary charge and the incident light flux) is generally very low (in the 10^{-10}−10^{-4} range). Sub-band gap photocurrent was attributed to optical transitions between delocalized band states and localized interfacial band gap states. This was supported by the fact that the yield depended on the electrolyte composition and on the pretreatment of the electrode surface. Chazalviel et al. found a huge increase in the sub-band gap photocurrent quantum yield of Si electrodes in acetonitrile solutions, when metal atoms and islands were deposited on the electrode surface. The quantum yield increased from about 10^{-7} with bare surfaces to about 10^{-3} for metalized surfaces. The sub-band gap photocurrent response was attributed to electron transitions mediated by (metal-induced) interfacial states distributed over a wide energy range in the band gap. Electrodes of nanoporous semiconductors (such as GaP and SiC) show a strong enhancement of the sub-band gap photocurrent quantum yield with respect to their nonporous counterparts.[6] Nanoporous semiconductors have a huge volume density of surface localized electrons,[7] and the absorption of photons mediated by interfacial band gap states is responsible for the enhanced quantum yield. With GaP photoanodes,[6] the sub-band gap photocurrent quantum yield increases with increasing temperature indicating that thermal excitation of electrons is involved in free carrier generation. Perhaps, the best known example of photocurrent generation induced by light absorption by surface-localized electrons is the dye-sensitized nanoporous TiO_2 electrode which forms the basis of the Grätzel-type solar cell.[8]

The occurrence of sub-band gap photocurrent in diode-type semiconductor devices with localized band gap states in, or at the edge of, the active layer of the system is well established. However, a comprehensive treatment of the mechanisms and the kinetics of electron−hole generation induced by sub-band gap optical transitions has not been presented. In this paper, we consider the main mechanisms which might be responsible for free carrier generation and photocurrent flow induced by absorption of sub-band gap photons. These mechanisms involve optical and thermal electronic transitions coupled by localized states in the band gap. The photocurrent quantum yield is calculated for each mechanism. Such a treatment reveals the parameters which determine the photocurrent quantum yield. However, it has become clear that a study of the mechanisms

S1089-5647(98)01252-8 CCC: $15.00
Published on Web 09/22/1998

and kinetics of free carrier generation induced by sub-band gap light requires the measurement of the sub-band gap photocurrent response due to modulation or perturbation of an important parameter.[9] We have calculated the photocurrent response due to harmonic modulation of the incident sub-band gap light intensity. It will be shown that analysis of the frequency or time-resolved sub-band gap photocurrent response enables one to distinguish between different mechanisms. Moreover, analysis of the photocurrent response under varying conditions of temperature and photon energy can be used to study the characteristics of the mediating band gap states. The analysis for the steady state holds, in principle, for any diode-type semiconductor device in which electrons and holes are separated. The analysis of the time-resolved photocurrent response holds for the case that the photocurrent corresponds to the movement of free electrons through the retrieval layer. A more general analysis is beyond the scope of this paper. We will present experimental results obtained with a photoelectrochemical cell, based on a nanoporous n-type GaP working electrode. The GaP anode (band gap 2.25 eV) is illuminated with 1.96 eV light from a He−Ne laser, modulated in intensity. It is shown that two mechanisms contribute to free carrier generation and that the characteristics of the mediating band gap states can be revealed by sub-band gap intensity modulated photocurrent spectroscopy.

Mechanisms of Free Carrier Generation Induced by Absorption of a Sub-Band Gap Photon

The main mechanisms of generation of a free electron in the conduction band and a free hole in the valence band induced by absorption of a sub-band gap photon are depicted in Figure 1a−e. These mechanisms involve optical and thermal transitions between the delocalized states in the valence and conduction bands and localized band gap states. Localized band gap states can be present in the bulk solid or at the interface. The mechanisms of free carrier generation may lead to sub-band gap photocurrent flow in insulators and in n- and p-type semiconductors if there is a retrieval layer in which electrons and holes are effectively separated. (For example, a single-crystal semiconductor electrode may have a retrieval region nearby the interface which consists of the depletion layer and the diffusion layer of the minority charge carrier, while in a p−i−n junction electrons and holes are separated in the entire intrinsic layer.) It is assumed that the localized states are distributed in energy in the gap; the density of states per energy unit will be denoted as $s(E)$. Although it is not necessary to specify the energy distribution in detail, it will be assumed here that the distribution of states in the gap does not show sharp peaks in limited energy regions. In mechanism a, an electron in the valence band (formally at energy $E - h\nu$) absorbs a photon (energy $h\nu$) and is promoted to a localized state at energy E in the gap. The rate of the optical transition per unoccupied band gap state at energy E is given by the probability of optical transition between the state at $E - h\nu$ and E, $k(E - h\nu,E)$, times the light intensity Φ. The hole formed at $E - h\nu$ relaxes very fast to the top of the valence band (energy E_v) and diffuses away. In mechanism a it is assumed that the electron, localized in the band gap state at energy E, is thermally excited to an energy level E' in the conduction band. This process is thermally activated with an activation energy $E' - E$. It is, therefore, reasonable to assume that thermal activation to the bottom of the conduction band (energy E_c) is dominant. The rate of thermal excitation of an electron from a band gap state at E to the bottom of the conduction band will be denoted as

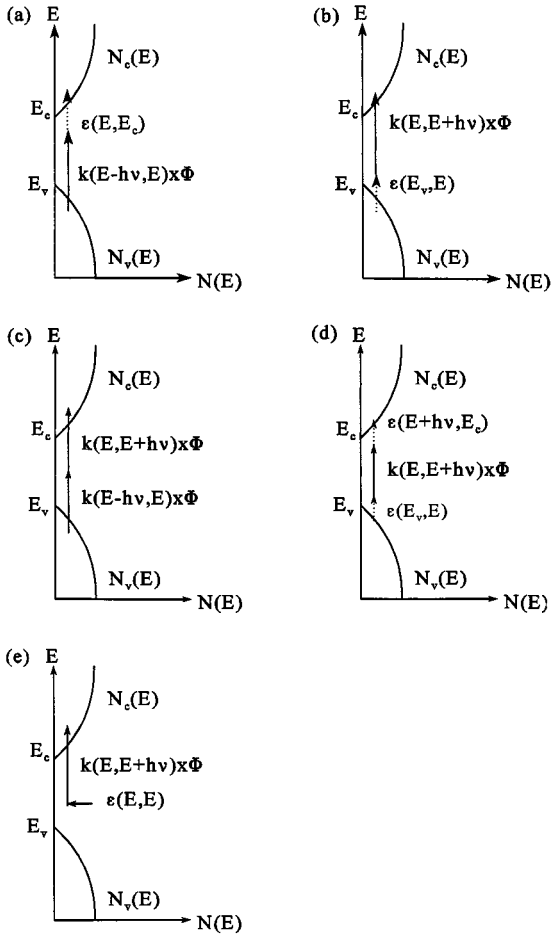

Figure 1. Mechanisms of electron−hole pair generation induced by absorption of a sub-band gap photon, mediated by localized band gap states. The vertical arrow ↑ indicates an optical transition from a delocalized state to a localized band gap state and vice versa; in mechanism d the optical transition involves two band gap states. The dotted vertical arrow indicates a thermal transition from a band gap state to a delocalized state or vice versa. In (e), states are filled due to interfacial electron transfer (horizontal arrow). Further explananation is given in the text.

$\epsilon(E,E_c)$. From detailed balance considerations it follows that $\epsilon(E,E_c)$ equals $\beta_n N_c \exp[(E - E_c)/k_B T]$, where β_n is the rate constant for the capture of a conduction band electron in a band gap state and N_c the effective density of states at the bottom of the conduction band.[10] By the combination of an optical transition (involving a sub-band gap photon) and a thermal transition, a free electron and hole are formed. If this occurs in the retrieval region of a semiconductor device, a steady-state photocurrent will flow in the external circuit. Moreover, the combination of an optical and thermal release process may induce a time lag between photon absorption and electron−hole pair generation.

In mechanism b, an electron from a localized state in the band gap at energy E is optically excited into the conduction band; the rate of this process per filled band gap state at E is denoted as $k[E,E + h\nu]\ \Phi$. The state in the band gap can be refilled with an electron from the valence band. Thermal excitation from the top of the valence band will be dominant. The rate per empty band gap state is denoted as $\epsilon(E_v,E)$. Similar to mechanism a, an electron−hole pair is generated by a combination of an optical and a thermal process, mediated by a band gap state. It will be further be shown that, under certain conditions, it is possible to distinguish between the two mechanisms by time-resolved photocurrent measurements. In

mechanism c, an electron−hole pair is generated by a combination of two optical transitions. The rates of the optical transitions between the valence band and band gap states and between the band gap and conduction band states are denoted as $k(E - h\nu,E)\Phi$ and $k(E,E + h\nu)\Phi$, respectively. In principle, also an optical transition between two localized states with energy in the gap may eventually lead to the generation of an electron−hole pair. A possible mechanism is shown in Figure 1d. However, for a moderate density of localized states, the optical transition probability between two localized states will generally be much lower than between a delocalized band and a band gap state. We will, therefore, not consider mechanism d in any detail.

The mechanisms a−c can be mediated by localized states in the bulk or at an interface. However, interfacial band gap states might enhance the sub-band gap photocurrent by an alternative mechanism. This is shown in Figure 1e for an n-type semiconductor. A sub-band gap photon is absorbed by a surface localized electron which is injected into the conduction band. The empty state is refilled with an electron from the adjacent phase, the rate per empty state being denoted as $\epsilon(E,E)$. If the adjacent phase is an electrolyte solution, the state is refilled by an electrochemical process involving a reducing agent. The latter mechanism is responsible for the photocurrent in a dye-sensitized TiO_2 solar cell, proposed by O'Regan and Grätzel.[8]

Steady-State Photocurrent and Photocurrent Response Due to Harmonic Modulation of the Light Intensity

In the foregoing section it was discussed how absorption of a photon of energy lower than the band gap energy may lead to a free electron and hole. If the electrons and holes are separated effectively, a steady-state photocurrent can be measured in the external circuit. It is of interest to calculate the photocurrent quantum yield for the mechanisms considered above. Here, the photocurrent quantum yield is defined as the ratio of the photocurrent density i (measured in the external circuit) divided by the incident light flux Φ (of monochromatic light, corrected for reflection loss) times the elementary charge e. Since photocurrent generation by sub-band gap light involves the combination of optical and thermal electron transitions, it is clear that the measured photocurrent can show a time lag with respect to light absorption. We, therefore, calculated the harmonic photocurrent density response $i(\omega)$ due to a harmonically varying light intensity $\Phi(\omega)$ [equal to $\Phi_m \exp(\sqrt{-1}\omega t)$] which is superimposed on the background light intensity Φ. It will become clear that measurement of the opto-electrical transfer function, $i(\omega)/e\Phi(\omega)$, is a powerful tool for the study of the mechanism and kinetics of sub-band gap photocurrent generation.

We consider a semiconductor device in which there is a region of width L in which photogenerated electron−hole pairs are separated effectively. The discussion of the time- or frequency-resolved photocurrent will be confined to systems in which the time-resolved photocurrent corresponds to the movement of conduction band electrons in the retrieval region. Such a system is, for instance, an n-type single-crystal electrode where the processes, discussed above, occur at the surface or in the near-surface region. Also a porous, nanostructured electrode in which the photogenerated electrons are collected in the substrate and the holes transferred to the interpenetrated electrolyte solution obeys this condition. The semiconductor device is illuminated with monochromatic sub-band gap light. Such light is weakly absorbed; it will, therefore, be assumed that the absorption depth is much larger than the width of the retrieval layer L. This means that the spatial dependence of the light intensity in the retrieval region can be neglected [$\Phi(x = 0) = \Phi(x = L)$, further denoted as Φ]. The photocurrent density, according to a given mechanism, can be calculated by taking into account the rate equation for the free electrons, generated at a given place x in the retrieval region:

$$\mathrm{d}n(x,t)/\mathrm{d}t = g(\text{mechanism}, t, \Phi, ...) - \mathrm{d}j_n(x,t)/\mathrm{d}x \quad (1)$$

Here, g(mechanism, t, Φ, ...) is the generation rate of electrons by one of the mechanisms considered above and $j_n(x,t)$ the flux of electrons in the retrieval region. The steady-state photocurrent (due to a specific mechanism) follows from integration of $\mathrm{d}j_n(x)/\mathrm{d}x$ over the width of the retrieval layer:

$$i(\text{mechanism}, \phi, ...) = e\int_0^L \mathrm{d}[j_n(x)] = e\int_0^L g(\text{mechanism}, \phi, ...)\,\mathrm{d}x = eLg(\text{mechanism}, \phi, ...) \quad (2)$$

The harmonic photocurrent response $i(\omega)$ due to a harmonically varying light intensity $\Phi(\omega)$ can also be calculated from eq 1. If it is assumed that the transport of photogenerated electrons through the retrieval layer is sufficiently fast and, hence, does not lead to a phase shift between $i(\omega)$ and $\Phi(\omega)$, the harmonic photocurrent response is given by

$$i(\text{mechanism}, \omega, \phi, ...) = e\int_0^L g(\text{mechanism}, \omega, \phi, ...)\,\mathrm{d}x = eLg(\text{mechanism}, \omega, \phi, ...) \quad (3)$$

Here, the steady-state photocurrent quantum yield and the harmonic photocurrent response will be calculated for mechanism a; see Figure 1a. The generation rate of electrons in the conduction band according to mechanism a is given by

$$g(\text{mechanism a}, \Phi(t), ...) = \int_{E_v}^{E_c} s(E)\,\epsilon(E,E_c)\,f(E,t)\,\mathrm{d}E \quad (4)$$

The electron occupation factor of the band gap states, $f(E,t)$, according to mechanism a is determined by

$$\mathrm{d}f(E,t)/\mathrm{d}t = k(E - h\nu,E)\,\Phi(t)\,[1 - f(E,t)] - \epsilon(E,E_c)\,f(E,t) \quad (5)$$

It follows that, under steady-state conditions, $f(E)$ is given by

$$f(E) = k(E - h\nu,E)\Phi/[k(E - h\nu,E)\Phi + \epsilon(E,E_c)] \quad (6)$$

When a harmonically varying light intensity, $\Phi(\omega)$ (of sufficiently small amplitude), is superimposed on the background light intensity, the occupation factor of the band gap states will show a harmonically varying part too, $f(E,\omega)$, which may show a phase shift with respect to $\Phi(\omega)$ due to the limited rate of thermal electron transitions. In the case of mechanism a, $f(E,\omega)$ can be calculated from eq 5. Using also eq 6, it is found that

$$\chi(\omega,E) = [f(E,\omega)/f(E)]/[\Phi(\omega)/\Phi] = \epsilon(E,E_c)/[\sqrt{-1}\omega + k(E - h\nu,E)\Phi + \epsilon(E,E_c)] \quad (7)$$

The complex transfer function $\chi(\omega,E)$ determines the photocurrent response due to a (small) perturbation or modulation of the sub-band gap light intensity. It will be shown further that $\chi(\omega,E)$ is characteristic for the mechanism of sub-band gap photocurrent generation. The steady-state sub-band gap photocurrent quantum yield according to mechanism a follows from eqs 2, 4, and 6

$$\frac{i}{e\Phi} = L\int_{E_v}^{E_c}\frac{i(E)}{e\Phi}\,dE \tag{8}$$

in which the contribution to the sub-band gap photocurrent quantum yield from states of energy E in the gap is given by

$$i(E)/e\Phi = s(E)\,[k(E - h\nu,E) + \epsilon(E,E_c)/\Phi]\,f(E)\,[1 - f(E)] \tag{9}$$

The harmonic photocurrent response due to modulation of the light intensity can be calculated from eqs 3, 4, and 7. For convenience, the result will be expressed as the opto-electrical transfer function, $i(\omega)/e\Phi(\omega)$, given by

$$\frac{i(\omega)}{e\Phi(\omega)} = L\int_{E_v}^{E_c}\left[\frac{i(E)}{e\Phi}\right]\chi(\omega,E)\,dE \tag{10}$$

This transfer function can be considered as the ac counterpart of the steady-state photocurrent quantum yield.

Equation 9 shows that the contribution to the steady-state sub-band gap photocurrent quantum yield of states at a given energy E is determined by $s(E)\,f(E)\,[1 - f(E)]$. This means that, even when the density of the mediating band gap states is a rather smooth function of the energy, the main contribution to the photocurrent quantum yield comes from states in a small energy range where $f(E) \approx {}^1/_2$. This can be rationalized with the following argument. It is assumed that the probability of the optical transition of a valence band electron at $E - h\nu$ to a band gap state at E does not depend strongly on E. The rate of optical filling of the band gap states by light of energy $h\nu$ and intensity Φ, i.e., $k(E - h\nu,E)\Phi$, will gradually decrease with increasing E in the forbidden gap, due to a decrease in the density of valence band states with increasing $E - h\nu$ toward the top of the valence band. Since optical transitions between two band gap states are very improbable, $k(E - h\nu,E)$ is nearly zero for states in the energy range between $E_v + h\nu$ and E_c. The rate $\epsilon(E,E_c)$ of the thermal transition of an electron from a state at energy E in the forbidden gap to the bottom of the conduction band increases *exponentially* with E increasing toward E_c. Therefore, the function $f(E)[1 - f(E)]$ shows a sharp peak around the energy at which $k[E - h\nu,E]\Phi = \epsilon(E,E_c)$; hence $f(E) = {}^1/_2$. With sufficiently high light intensity, the maximum in $f(E)[1- f(E)]$ is found close to $E = E_v + h\nu$. It then follows that the photocurrent quantum yield and the opto-electrical admittance are dominated by states in a small energy region (width $4k_BT$) around $E = E_v + h\nu$. Equation 8 can then be simplified to

$$i/e\Phi \approx L(k_BT)\,s(E = E_v + h\nu)\,k(E_v,E_v + h\nu) \tag{8b}$$

and the opto-electrical transfer function to

$$\frac{i(\omega)}{e\Phi(\omega)} \cong \frac{i}{e\Phi}\chi(\omega, E = E_v + h\nu) = \frac{i}{e\phi}\,\frac{\epsilon(E_v + h\nu, E_c)}{\sqrt{-1}\omega + 2\epsilon(E_v + h\nu, E_c)} \tag{10b}$$

From eqs 7 and 10b, it follows that a plot of the opto-electrical transfer function according to mechanism a in the complex plane is a semicircle in the [Re = pos, Im = neg] quadrant (see Table 1). The low-frequency limit is a value on the real axis equal to the half of the steady-state sub-band gap photocurrent quantum yield. The high-frequency limit is zero. The characteristic frequency, ω_a, of the semicircle is given by $2\epsilon(E = E_v + h\nu,E_c)$ equal to $2\beta_nN_c\exp[(E_v - E_c + h\nu)/k_BT]$. The evolution of the transfer function in the frequency domain can be rationalized by a reasoning in the time domain. Consider a sub-band gap light pulse starting at time $t = 0$. Since, here, the time-resolved photocurrent response is due to the movement of free electrons in the retrieval region, mechanism a will lead to a photoinduced electrical signal as soon as the electrons, being optically excited from the valence band into a band gap states, are thermally excited into the conduction band. Hence, the photocurrent lags behind the onset of the light pulse. The attenuation between photocurrent and light pulse is determined by the rate of thermal excitation of electrons from states in the band gap into the conduction band.

The steady-state photocurrent quantum yield and the opto-electrical transfer function can be calculated for the mechanisms b, c, and e in a similar way. For each mechanism, the steady-state photocurrent quantum yield can be described by eq 8, with a specific expression for $i(E)/e\Phi$, summarized in Table 1. The opto-electrical transfer function can formally be described by eq 10 with the function $\chi(\omega,E)$ being specific for a given mechanism (see Table 1).

It can be seen that the contribution to the steady-state photocurrent quantum yield and the opto-electrical transfer function of band gap states at energy E is proportional to the product $f(E)[1 - f(E)]$. For the mechanisms a and b, in which one of the charge carriers is thermally excited from a band gap state to a delocalized state, $f(E)[1 - f(E)]$ will show a sharp maximum as a function of E. Mainly states at energy around $E_v + h\nu$ will be involved in mechanism a while states around $E_c - h\nu$ will be involved in mechanism b. In the case of mechanism c (consecutive absorption of two photons), $f(E)[1 - f(E)]$ is expected to show a relatively broad peak with maximum around midgap. Finally, all band gap states in the energy range above $E_c - h\nu$ can be involved in mechanism e if refilling of the interfacial state is sufficiently fast.

It is clear that the different mechanisms can be distinguished on the basis of the opto-electrical transfer function; for convenience plots of $\chi(\omega,E)$ in the complex plane with the measuring frequency ω as a parameter are also shown in Table 1. The function $\chi(\omega,E)$ is plotted for the energy range for which the largest contribution to the sub-band gap photocurrent quantum yield is expected (the energy range where $f(E) \approx {}^1/_2$). The formulas for the steady-state quantum yield corresponding to mechanisms a and b are formally the same and do not allow a distinction to be drawn. However, the evolution of $\chi(\omega,E)$ and hence of the opto-electrical transfer function in the frequency domain are completely different.

Sub−Band Gap Intensity Modulated Photocurrent Spectroscopy with Nanoporous GaP Electrodes

In this section it will be shown that the mechanism(s) of photocurrent generation in nanoporous n-type GaP electrodes can be studied by intensity modulated photocurrent spectroscopy and that the results obtained with this method can be interpreted quantitatively within the theoretical framework which was presented in the previous section.

A nanoporous GaP network can be prepared by anodic etching of single crystalline n-type GaP electrodes at a sufficiently positive electrode potential. Much research has been devoted to study of the morphology and structure of nanoporous GaP and the opto-electric properties.[6a,b] A SEM photograph is presented in Figure 2. It can be seen that the GaP network, formed by anodic etching under dielectric breakdown conditions, consists of strongly interconnected structural units with dimensions in the 100 nm range. By use of Raman spectroscopy it

TABLE 1: Contribution $i(E)/e\Phi$ to the Photocurrent Quantum Yield for States with a Density $s(E)$ in the Band Gap and the Complex Function $\chi(\omega,E)$ determining the Opto-Electrical Transfer Function for Different Mechanisms of Free Carrier Generation Induced by Sub-Band Gap Light[a]

	$i(E)/e\Phi$	$\chi(\omega,E)$	
(a)	$s(E)\,[k(E-h\nu,E) + \varepsilon(E,E_C)/\Phi]\times$ $f(E)\,[1-f(E)]$	$\dfrac{\varepsilon(E,E_C)}{\sqrt{-1}\,\omega + k(E-h\nu,E)\,\Phi + \varepsilon(E,E_C)}$	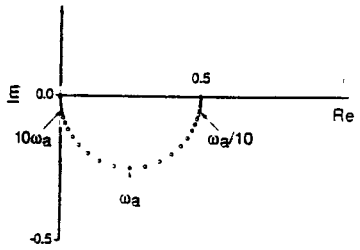
(b)	$s(E)\,[k(E,E+h\nu) + \varepsilon(E_V,E)/\Phi]\times$ $f(E)\,[1-f(E)]$	$\dfrac{\sqrt{-1}\,\omega + \varepsilon(E_V,E)}{\sqrt{-1}\,\omega + k(E,E+h\nu)\,\Phi + \varepsilon(E_V,E)}$	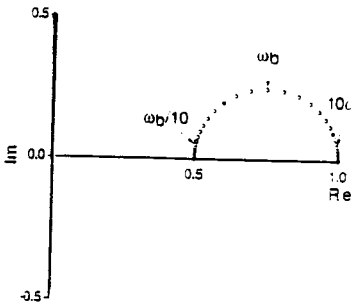
(c)	$s(E)\,[k(E-h\nu,E) + k(E,E+h\nu)]\times$ $f(E)\,[1-f(E)]$	1	
(e)	$s(E)\,[k(E,E+h\nu) + \varepsilon(E,E)/\Phi]\times$ $f(E)\,[1-f(E)]$	$\dfrac{\sqrt{-1}\,\omega + \varepsilon(E,E)}{\sqrt{-1}\,\omega + k(E,E+h\nu)\,\Phi + \varepsilon(E,E)}$	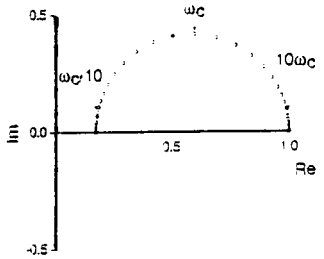

[a] The labels *a, b, c, e* refer to the different mechanisms discussed in the text and sketched in Figure 1. A plot of $\chi(\omega,E)$ (for half-filled band gap states) in the complex plane with the measuring frequency ω as a parameter is also shown.

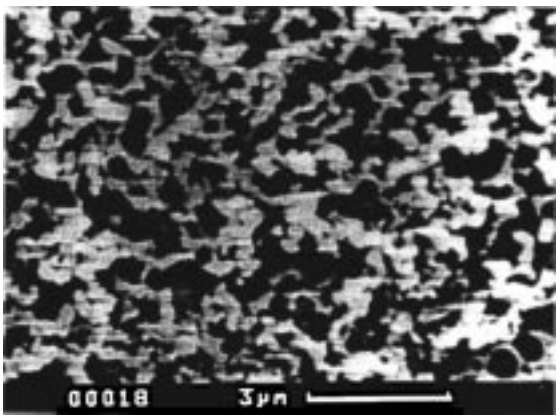

Figure 2. SEM photograph of a nanoporous GaP network. The network consists of strongly interconnected units with dimensions in the 100 nm range.

has been shown that such a nanoporous GaP network is still crystalline.[11] From luminescence measurements it followed that the GaP structures are not size-quantized.[6a] The photoelectrochemical properties of nanoporous GaP electrodes were shown to be very interesting. The photocurrent quantum yield with indirectly absorbed light ($2.25 < h\nu < 2.76$ eV) was found to be close to unity. This is about 100 times larger than for single-crystal electrodes. This phenomenon could be rationalized by the fact that the width of the retrieval layer (in which electron−hole pair separation is fully effective) is about equal to the typical dimensions of the porous structure (in the 100 nm range; see Figure 2). This means that all minority carriers (holes) generated in the porous structure will reach the interface and, hence, be saved from recombination in the bulk. The time-resolved photocurrent measured in the external circuit is due to the movement of photogenerated free electrons, in agreement with the assumption made in the theory section. It was observed that the photocurrent quantum yield with light of energy below the band gap (2.25−1.9 eV) was still reasonably large (between 0.1 and 0.001) and showed an increase proportional to the thickness of the porous film. The largely increased quantum yield for sub-band gap photocurrent is attributed to the fact that the entire porous network (characterized by a huge density of interfacial states) absorbs sub-band gap light and is active in electron−hole pair separation. A remarkable enhancement of the sub-band gap photocurrent quantum yield by porous etching was also observed with SiC electrodes.[6c] The fact that free carriers are generated with sub-band gap light is further illustrated with results presented in Figure 3, where the open-circuit potential of a nanoporous GaP electrode is shown as a function of the incident intensity of 1.96 eV light from a He−Ne laser. The open-circuit potential becomes gradually more negative with increasing light intensity. This shows that absorption of 1.96 eV light leads to an increase of the Fermi level in the nanoporous electrode beyond the dark (equilibrium) level; this means that steady-state illumination with sub-band

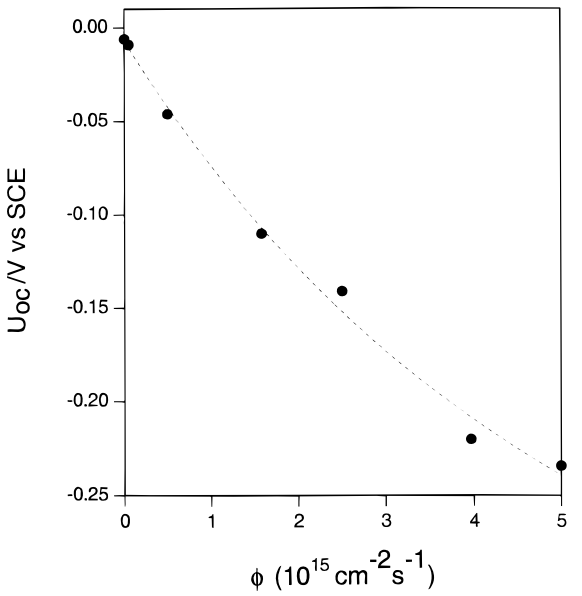

Figure 3. Open-circuit potential, U_{oc}, of a nanoporous GaP electrode in aqueous electrolyte (1 M H_2SO_4) as a function of the incident intensity of sub-band gap light (1.96 eV) from a He−Ne laser.

gap light shifts the generation−recombination equilibrium to a steady state characterized by a higher concentration of free electrons.

The mechanism of free carrier generation induced by absorption of 1.96 eV light has been investigated by IMPS. Nanoporous GaP films of thickness between 10 and 50 μm were prepared on crystalline GaP substrates by anodic etching. Such electrodes were used as working electrodes in a conventional three-electrode electrochemical cell, using an EG&G 273A potentiostat. The electrode was illuminated from the electrolyte side with 1.96 eV light from a He−Ne laser, and the steady-state sub-band gap photocurrent and harmonic photocurrent response were measured under potentiostatic conditions. The light intensity was modulated (10% depth) with an acousto-optic modulator, the frequency $\omega/2\pi$ was varied between 10^{-1} and 10^4 Hz. The opto-electrical transfer function, $i(\omega)/e\Phi(\omega)$, was measured by using a beam splitter, a fast silicon photodiode, and a frequency response analyzer (Solartron 1255). More details dealing with IMPS can be found elsewhere.[12] Measurements were performed in acid aqueous solutions at different temperatures (between 0 and 50 °C). It was found previously that addition of H_2O_2 to the solution increases the sub-band gap photocurrent quantum yield considerably.[6b] Therefore, IMPS measurements were also performed in acid electrolytes with various concentrations of H_2O_2.

In Figure 4a,b, complex plane plots of the opto-electrical transfer function $i(\omega)/e\Phi(\omega)$ are presented in the frequency range between 2π 10^{-1} and 2π 10^4 rad s^{-1} for two porous GaP photoanodes. The electrode potential was at least 0.5 V more positive than the open-circuit potential; hence electron−hole recombination was (nearly) absent. Results are shown for different temperatures. In Figure 5, $i(\omega)/e\Phi(\omega)$ is presented in the complex plane, measured with a nanoporous GaP electrode immersed in an acidic aqueous solution with and without H_2O_2. Finally, in Figure 6, $i(\omega)/e\Phi(\omega)$ is shown measured with a porous GaP electrode in a solution of 0.5 M H_2SO_4 and 0.02 M H_2O_2 at four different temperatures.

Generally, $i(\omega)/e\Phi(\omega)$ shows two features in the [Re = pos, Im = neg] quadrant. In the lower frequency region, a (somewhat flattened) semicircle is observed. From Figure 5,

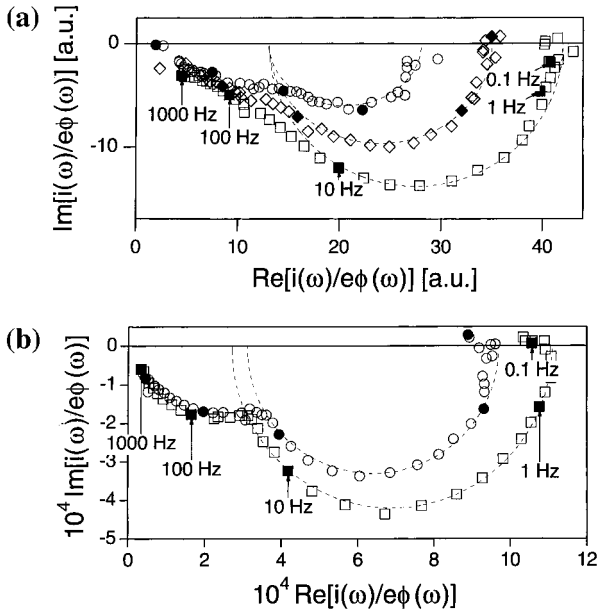

Figure 4. (a) Complex plane plot of the opto-electrical transfer function, $i(\omega)/e\Phi(\omega)$, with the modulation frequency ω as a parameter. The measurements were performed with a nanoporous n-GaP photoanode (thickness of porous film being 50 μm) in aqueous electrolyte (1 M H_2SO_4), at a potential of 0.2 V vs SCE. Intensity-modulated He−Ne laser light ($h\nu$ = 1.96 eV) was used; the background light intensity was 5×10^{15} cm^{-2} s^{-1}. Plots are shown for three different temperatures: (○) 275 K; (◇) 303 K; (□) 322 K. (The data according to $\omega/2\pi$ = 0.1 Hz, 1 Hz, 10 Hz, ... are indicated with filled symbols.) (b) Complex plane plot of the opto-electrical transfer function, $i(\omega)/e\Phi(\omega)$, with the modulation frequency ω as a parameter. The measurements were performed with a nanoporous n-GaP photoanode (thickness of porous film 10 μm) in aqueous electrolyte (1 M H_2SO_4), at a potential of 1.0 V vs SCE. Intensity-modulated He−Ne laser light ($h\nu$ = 1.96 eV) was used. Plots are shown for two different temperatures: (○) 283 K; (□) 323 K. (The data according to ω /2π = 0.1 Hz, 1 Hz, 10 Hz, ... are indicated with filled symbols.)

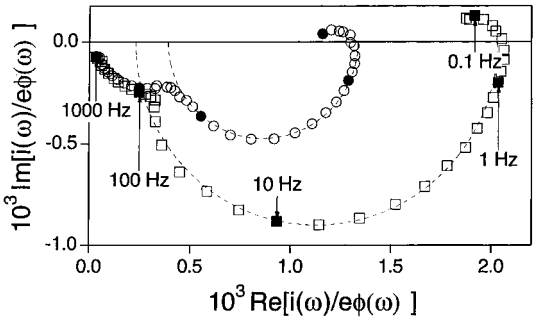

Figure 5. Complex plane plot of the opto-electrical transfer function, $i(\omega)/e\Phi(\omega)$, with the modulation frequency ω as a parameter. The measurements were performed with a nanoporous GaP photoanode (thickness of porous film 10 μm) in aqueous electrolyte (0.5 M H_2SO_4) with and without H_2O_2: (○) no H_2O_2; (○) 0.02 M H_2O_2. The electrode potential was 1.0 V, and the temperature, 295 K. Intensity-modulated He−Ne laser light ($h\nu$ = 1.96 eV) was used.

it can be seen that the radius of the low-frequency semicircle increases considerably when H_2O_2 is added to the electrolyte. From Figure 4a,b (results without H_2O_2) and Figure 6 (results with H_2O_2), it can be seen that the diameter of the low-frequency semicircle increases with increasing temperature. It was also found that the characteristic frequency of the low-frequency semicircle (this is the frequency for which the imaginary component is most negative, further denoted as ω_m) increases considerably with increasing temperature. The characteristic frequency is plotted vs the temperature in Figure 7, as

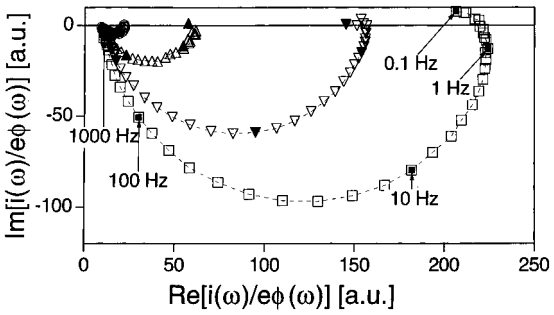

Figure 6. Complex plane plot of the opto-electrical transfer function, $i(\omega)/e\Phi(\omega)$, with the modulation frequency ω as a parameter. The measurements were performed with a nanoporous n-GaP photoanode (thickness of porous film being 25 μm) in aqueous electrolyte (0.5 M H_2SO_4 + 0.02 M H_2O_2), at a potential of 0.5 V vs SCE. Intensity-modulated He−Ne laser light ($h\nu = 1.96$ eV) was used. Plots are shown for four different temperatures: (○) 275 K; (△) 293 K; (▽) 311 K; (□) 321 K. (The data according to $\omega/2\pi = 0.1$ Hz, 1 Hz, 10 Hz, ... are indicated with filled symbols.)

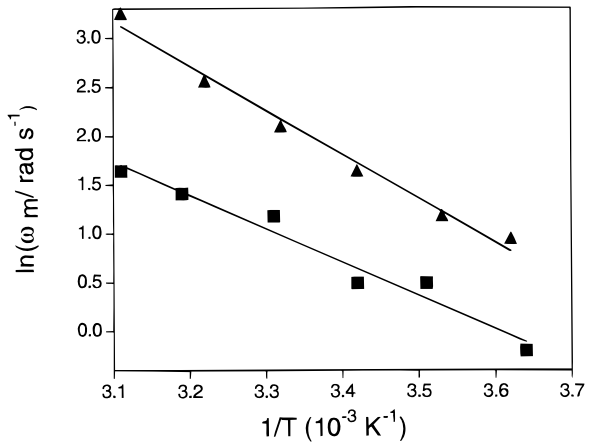

Figure 7. Plot of the characteristic frequency ω_a of the opto-electrical transfer function in the lower frequency region as $\ln(\omega_a/\text{rad s}^{-1})$ vs $1/T$ for the measurements in aqueous electrolyte (0.5 M H_2SO_4) (■) and with 0.02 M H_2O_2 added to the electrolyte (▲).

$\ln(\omega_m/\text{rad}\cdot\text{s}^{-1})$ vs $1/T$, for measurements performed in an acidic electrolyte, with and without H_2O_2 present. A linear relationship is found in both cases. By averaging the results obtained with 4 different samples, we obtained the "activation energy" of ω_m being 0.3 eV ± 0.05 eV in acid electrolyte and 0.4 eV ± 0.05 eV if H_2O_2 was present.

Generally, the high-frequency limit of *the low-frequency semicircle* indicates a value above zero, which shows that there is a second contribution to the sub-band gap photocurrent. From Figures 4 and 5 it can be seen that, at higher frequencies, there is a second feature in the plots of $i(\omega)/e\Phi(\omega)$ in the complex plane. Analysis of a large amount of data obtained at different temperature using acidic solutions with and without H_2O_2 showed that the second contribution to the photocurrent is independent of temperature (in the range 0−50 °C) and not influenced by the presence of H_2O_2 in the solution.

The two features observed in the opto-electrical transfer function indicate that free carrier generation is due to two different mechanisms. A comparison with the theory (see Table 1) shows that the low-frequency semicircle corresponds to mechanism a. Indeed, the low-frequency semicircle is situated in the [Re = pos, Im = neg] quadrant and reflects a thermally activated process. Accordingly, the characteristic frequency should correspond to two times the rate of thermal excitation of an electron, localized in a band gap state, into the conduction band, i.e. $2\epsilon(E,E_c)$ which is equal to $2\beta_n N_c \exp[(E - E_c)/k_BT]$ (see eq 10b). It is shown in the theoretical section that, if the energetic distribution of localized states in the band gap does not show sharp peaks, the states with energy around $E_v + h\nu$ will give the largest contribution to the sub-band gap photocurrent via mechanism a. As the energy of the photons is 1.96 eV and the band gap is 2.25 eV, the states situated about 0.3 eV below the conduction band are expected to be dominant in mechanism a; the activation energy is expected to be 0.3 eV. This is in agreement with the experimental results obtained in acidic electrolytes without H_2O_2 (see Figure 7). From the results it follows that the sub-band gap photocurrent in the presence of H_2O_2 is considerably larger and that this is due to a larger contribution via mechanism a. It is reported in the literature that H_2O_2 chemisorbs on the surface of III−V semiconducting compounds.[13] It is hence reasonable to assume that in the case of nanoporous GaP *interfacial* band gap states are involved in sub-band gap photocurrent generation via mechanism a and that chemisorbed H_2O_2 increases the density of interfacial states in the appropriate energy region considerably. The activation energy for thermal electron excitation into the conduction band is found to be 0.4 eV in the presence of H_2O_2; this is about 0.1 eV larger than expected from the theory and observed in acidic electrolytes without H_2O_2. This indicates that chemisorbed H_2O_2 induces states with a relatively sharp distribution about 0.4 eV below the conduction band.

The results show that there is a second contribution to the sub-band gap photocurrent in GaP. This contribution is independent of the temperature and is not affected by the presence of a hole scavenger (such as Fe^{2+}) nor by adsorption of H_2O_2. The second contribution must be attributed to two consecutive optical transitions, involving delocalized states in the valence band, localized states situated around midgap, and delocalized states in the conduction band (i.e. mechanism c). The fact that the second contribution is not influenced by the electrolyte composition strongly suggests that localized bulk states are involved. According to the theory, the contribution to the sub-band gap photocurrent by mechanism c should not be attenuated with respect to light absorption (see Table 1; $\chi(\omega,E) \equiv 1$). In some cases, a semicircle is found at higher frequencies, with a characteristic frequency around 10^3 rad s^{-1}. However, this behavior is also found when nanoporous GaP is illuminated with intensity modulated, directly absorbed UV light[14] and reflects the slow diffusive transport of photogenerated electrons through the porous network toward the substrate (under full depletion) or the photoinduced RC-discharge of the GaP photoanode (under weak depletion). It is remarked here that free carrier generation by consecutive absorption of two photons, mediated by midgap states, has also been observed with single-crystal SiC electrodes.[5d]

It can be concluded that IMPS with 1.96 eV sub-band gap light shows that there are two contributions to sub-band gap photocurrent generation in nanoporous GaP photoanodes. A small contribution results from two consecutive optical transitions involving band gap states in the bulk. The dominant contribution results from an optical transition from delocalized states at (the top of) the valence band to localized states 0.3−0.4 eV below the bottom of the conduction band, followed by a thermal transition from these states to the (bottom of) the conduction band. The dominant contribution is strongly enhanced if H_2O_2 is chemisorbed on the GaP surface.

Finally, we consider how far sub-band gap IMPS can be used to characterize localized band gap states. It must be stressed here that several methods using sub-band gap light have been

proposed and used to characterize band gap states in single crystals.[3,4] These methods are based on a single optical transition between a band and (surface-) localized band gap states. For instance, surface photovoltage spectoscopy was introduced by Gatos and co-workers[4a] and successfully used for characterization of semiconductor surfaces. This method is based on measurement of the photovoltage due to majority carriers generated by sub-band gap optical transitions. Basically, the energy of the sub-band gap light is varied, and surface states confined to a small energy region can be characterized. It is however clear that interpretation of results obtained with this method becomes more difficult if surface states are present in several energy regions in the gap or if surface states show a broad distribution in the gap. Our work shows that the coupling of an optical and thermal transition (such as in mechanisms a and b) in free carrier generation may confine the energy range of the mediating band gap states to a predictable energy region of some k_BT. Typically, states around $E_v + h\nu$ and $E_C - h\nu$ can be characterized. If electrons and holes are generated by two consecutive optical transitions, predominantly states around midgap will be involved. In the case of n-type GaP (band gap is 2.25 eV) probed with photons of 1.96 eV, interfacial states about 0.3 eV below the band gap are involved in free carrier generation via mechanism a. According to our model, the characteristic frequency of the opto-electrical transfer function corresponds to $2\epsilon(E_v + 1.96\ \text{eV},E_c)$ equal to $2\beta_n N_c \exp[-0.3\ \text{eV}/k_BT]$, where β_n is the rate constant for electron capture by the mediating interfacial states. Hence, a value for β_n can be estimated from extrapolation of the plots presented in Figure 7 to $1/T \equiv 0$. Values for β_n between 10^{-13} and 10^{-15} $cm^3\ s^{-1}$ are found for nanoporous GaP in acidic electrolytes. A much more reproducible value of nearly 10^{-12} $cm^3\ s^{-1}$ was found if H_2O_2 was chemisorbed on the GaP surface. Chemisorption of H_2O_2 not only enhances the density of interfacial states but, apparently, also leads to a higher value of the electron capture rate constant of the interfacial states. Probably, chemisorbed H_2O_2 gives rise to a strongly polar surface entity. This type of surface species is believed to play a key role in the electrochemistry and surface chemistry of III−V semiconductors in H_2O_2-containing solutions.[13] For instance, during chemical etching of n-type GaAs single crystals in H_2O_2 containing solutions an anodic current due to electron injection from an intermediate species in the etching process is observed.[13]

References and Notes

(1) Pankove, J. I. *Optical processes in semiconductors*; Prentice-Hall: Englewood Cliffs, NJ, 1971.

(2) (a) Street, R. A. *Hydrogenated Amorphous Silicon*; Cambridge Solid State Science Series; Cahn, R. W., Davis, E. A., Ward, I. M., Eds.; Cambridge University Press: New York, 1991. (b) Carasco, F.; Spear, W. E. *Philos. Mag. B* **1983**, *47*, 495.

(3) Chiarotti, G.; Del Signore, G.; Nannarone, S. *Phys. Rev. Lett.* **1968**, *21*, 1170.

(4) (a) Lagowski, J. *Surf. Sci.* **1994**, *299/300*, 92. (b) Bube, R. H.; Cardon, F. *J. Appl. Phys.* **1964**, *35*, 2712. (c) Evwaraye, A. O.; Smith, S. R.; Mitchel, W. C. *J. Appl. Phys.* **1995**, *77*, 4477. (d) Semaltianos, N. G.; Karczewski, G.; Hu, B.; Wojtowicz, T.; Furdyna, J. K. *Phys. Rev. B* **1995**, *51*, 17499.

(5) (a) Beckmann, K. H.; Memming, R. *J. Electrochem. Soc.* **1969**, *116*, 368. (b) Chazalviel, J.-N.; Stefenel, M.; Truong, T. B. *Surf. Sci.* **1983**, *134*, 865. (c) Nogami, G.; Okhubo, S.; Avalle, L.; Hongo, K. *J. Electrochem. Soc.* **1996**, *143*, 3600. (d) van de Lagemaat, J.; Vanmaekelbergh, D.; Kelly, J. J. Photoelectrochemical Characterization of 6H−SiC. *J. Appl. Phys.* **1998**, *83*, 6089.

(6) (a) Erné, B. H.; Vanmaekelbergh, D.; Kelly, J. J. *Adv. Mater.* **1995**, *7*, 739. (b) Iranzo Marín, F.; Hamstra, M. A.; Vanmaekelbergh, D. *J. Electrochem. Soc.* **1996**, *143*, 1137. (c) van de Lagemaat, J.; Plakman, M.; Vanmaekelbergh, D.; Kelly, J. J. *Appl. Phys. Lett.* **1996**, *69*, 2801.

(7) If it is assumed, for simplicity, that a nanostructured nanoporous semiconductor consists of closest-packed spheres of radius *r*, the volume density of surface atoms can be estimated from $\{[4\pi r^2]/[(4/3)\pi r^3]\}$ times (about) 10^{15} cm^{-2}. For systems assembled of spheres with radius of 100, 10, and 1 nm, the volume density of surface atoms is then about 10^{20}, 10^{21}, and 10^{22} cm^{-3}, respectively. For comparison, the density of GaAs units in single crystalline GaAs is about 10^{22} cm^{-3}.

(8) O'Regan, B.; Grätzel, M. *Nature* **1991**, *353*, 737.

(9) Vanmaekelbergh, D.; van Pieterson, L. *Phys. Rev. Lett.* **1998**, *80*, 821.

(10) Simmons, J. G.; Taylor, G. W. *Phys. Rev. B* **1971**, *4*, 502.

(11) Tiginyanu, I. M.; Ursaki, V. V.; Karavanskii, V. A.; Sokolov, V. N.; Raptis, Y. S.; Anastassakis, E. *Solid State Commun.* **1996**, *97*, 675.

(12) Peter, L. M. *Chem. Rev.* **1990**, *90*, 753.

(13) Minks, B. P.; Oskam, G.; Vanmaekelbergh, D.; Kelly, J. J. *J. Electroanal. Chem.* **1989**, *273*, 119.

(14) (a) Vanmaekelbergh, D.; Iranzo Marín, F.; van de Lagemaat, J. *Ber. Bunsen-Ges. Phys. Chem.* **1996**, *100*, 616. (b) de Jongh, P. E.; Vanmaekelbergh, D. *Phys. Rev. Lett.* **1996**, *77*, 3427.